Supporting Information:

In Situ Lithiation-Delithiation of Mechanically Robust Cu-Si Core-shell Nanolattices in a Scanning Electron Microscope

Xiaoxing Xia[*1], Claudio V. Di Leo[2], X. Wendy Gu[1,3], Julia R. Greer[1]*

[1] Division of Engineering and Applied Science, California Institute of Technology, 1200 E. California Blvd., Pasadena, CA 91125, United States

[2] School of Aerospace Engineering, Georgia Institute of Technology, 270 Ferst Drive, Atlanta, GA 30332, United States

[3] Department of Chemistry, University of California at Berkeley, 419 Latimer Hall, Berkeley, CA 94720, United States

Experiment Section

The Cu-Si core-shell nanolattices were fabricated by first making 3D polymer templates via two-photon lithography in a positive resist (Microchem AZ4620), electroplating Cu into the openings within this template, stripping the resist matrix, and then depositing a layer of a-Si onto the Cu scaffold by plasma enhanced chemical vapor deposition (PECVD). The photoresist was spincoated onto a 15nm Au-coated glass cover slip and cured at 110°C for 3min. Two-photon lithography (Nanoscribe, GmbH) was used to write the octet lattice structure designed in MatLab using laser powers in a range of 0.8-1.2mW and a writing speed of 10μm/s. The patterned photoresist was developed in a solution of AZ400k: DI water at 1: 4 ratio. Using the remaining photoresist matrix as a 3D template, galvanostatic Cu electrodeposition was conducted in a three-electrode setup with a Cu counter electrode and Ag/AgCl reference electrode. The electroplating bath was composed of 100g/l $CuSO_4 \cdot 5H_2O$, 200g/l H_2SO_4, and commercial Cu electroplating additives (5ml/l 205M, 1ml/l 205KA, and 1ml/l 205KR, Electrochemical Products, Inc). After electroplating, the photoresist matrix was removed by soaking in 1-methyl-2-pyrrolidone, leaving the freestanding Cu lattices on a Au thin film on a glass substrate. The Cu lattices had a ~20% variation in beam diameter for the range of lithography laser power used in this work. A layer of a-Si was then deposited on the Cu lattice scaffold by PECVD at 200°C with 5% silane precursor gas at 250sccm flow rate and 800mTorr pressure for 30min.

To analyze the microstructure of the Cu core, Si shell and the Cu-Si interface, we prepared a thin lamella of the Cu-Si beam cross-section using a SEM/FIB Dualbeam (Nova 600, FEI) and positioned it onto a TEM grid with a micromanipulator (Omniprobe). The final thinning step of the TEM sample was completed using 8keV Ga ion beam at 42pA to minimize beam damage. TEM analysis revealed the presence of a few, 20-30nm-sized voids located at the Cu-Si interface (Fig. 1f). Possible ion beam damage due to FIB was examined using the open source software package SRIM-The Stopping and Range of Ions in Solids (http://www.srim.org/), which conducts Monte Carlo simulation of the trajectory of implanted ion and recoiling target atom with full damage cascade. Fig. S1 shows the cross-sections of the interaction volume on Si and Cu target after 10000 8keV Ga ion bombardment, where x-axis is the depth in the target sample and y-axis is the coordinate on the target surface with Ga ion being implanted at y = 0. The red dots are those collisions between the ion and target atoms in which the target atoms are knocked from their lattice sites. The green dots are collisions between recoiling target atoms and other target atoms. The width and the depth of the Ga interaction volume of the Si target are both ~40nm (Fig. S1-a) and those of the Cu target are ~20nm (Fig. S1-c). During FIB milling, the amount of damage on the cross-sectional face in the lateral direction to the incident Ga beam is approximately half of the interaction volume on each side of the TEM lamella. The final TEM sample is approximate 80-100nm thick but the total damage region is about 40nm thick for Si and about 20nm thick for Cu. Therefore, we believe it is unlikely that the 20-30nm-sized voids at the Cu-Si interface found during TEM analysis were caused by FIB damage. It is worth mentioning that SRIM doesn't take into account any thermal effects, so the calculated ion damage is what would have happened at 0K. Implanting at room-temperature (300K) will cause most of the implantation damage to “self-anneal”. The target damage might disappear because at room temperature, the lattice atoms have adequate energy to allow simple target damage to regrow back into its original crystalline form. Furthermore, we used the Omniprobe to lift out a Cu beam before Si deposition and glued it sideways on the substrate with Pt deposition in the SEM (with the major axis of the elliptical beam cross-section parallel to the substrate). An atomic force microscope (AFM) was used to measure

the root-mean-square roughness of the Cu surface to be 22nm. We believe it is possible that the Cu surface roughness is what gave rise to the voids at the Cu-Si interface during Si deposition.

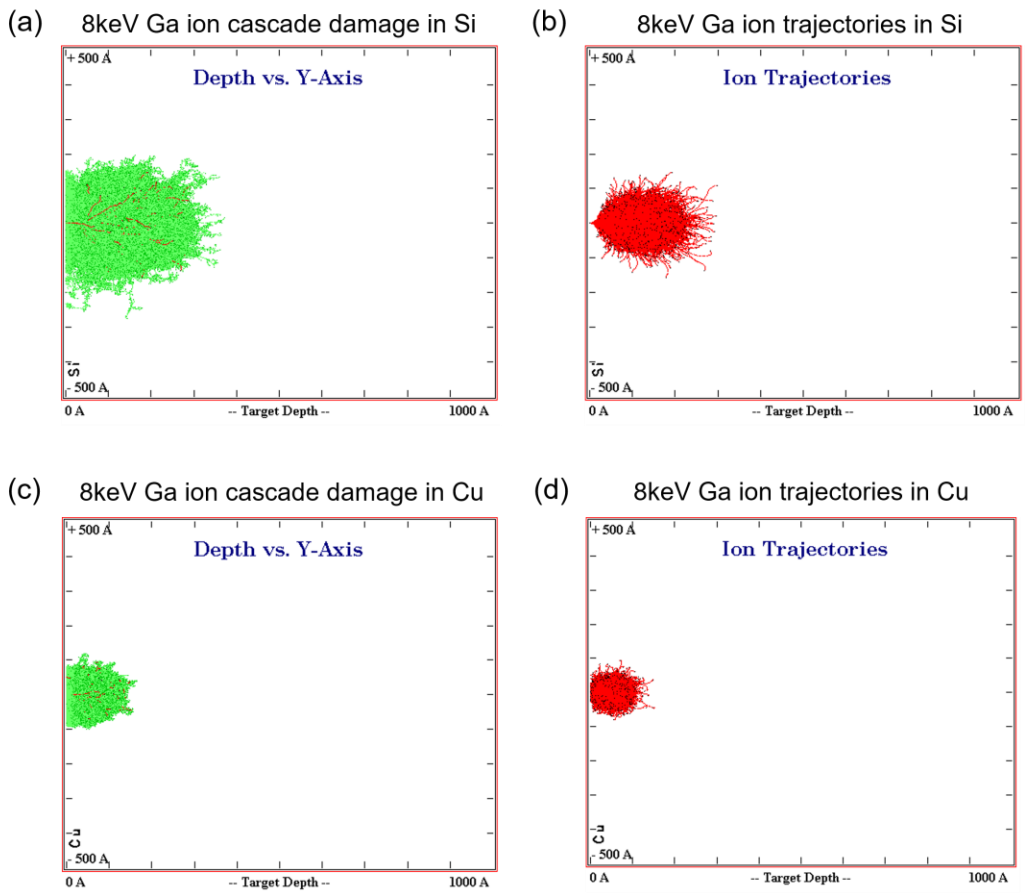

Figure S1. SRIM simulation results of 8keV Ga ion interaction volume in (a) Si and (c) Cu target and the Ga ion trajectories in (b) Si and (d) Cu target.

The volume of Cu and Si in the nanolattices was calculated using Solidworks, in which a model of a Cu-Si core-shell octet unit cell was created. The modeled Cu-Si beam has an elliptical cross-section (0.9µm minor axis and 2µm major) for the Cu core and a 250nm conformal coating of Si, and the model takes into account the volume in lattice beams and at lattice nodes. The Si volume in an 8µm unit cell is calculated to be 98µm^3, and the Cu volume is 122µm^3.

A custom-made lithiation setup was constructed by assembling an electrochemical half-cell with a Li counter electrode inside the vacuum chamber of an *in situ* SEM nanomechanical instrument (Quanta 200 SEM, FEI and Nanomechanics, Inc.). The electrochemical cell was connected to an external potentiostat. The glass substrate supporting the Cu-Si core-shell nanolattices was held vertically on the side of a SEM sample holder. A ~500µm–diameter piece of Li was attached to a W tip inside of a glovebox, transferred to the SEM in an Ar-filled container and then quickly mounted onto the nanomechanical arm inside the SEM chamber with less than 10s exposure in air. The negative electrode of the potentiostat was connected to the Li electrode via the W tip, and the positive electrode of the potentiostat was connected to the Au film on the sample substrate. We aligned the Li electrode to be positioned directly above the Cu-Si nanolattice in the SEM image.

The Li electrode can be lowered to form a half-cell, in which either solid Li_2O or 10wt% LiTFSI in P_{14}TFSI ionic liquid was used as the electrolyte. The lithiation rate C_{rate} is the rate of discharge defined by the multiplicative inverse of the number of hours it takes to fully discharge an electrochemical cell based on the theoretical capacity of Si (i.e. 0.25C indicates a full discharge in 4hr). Fig. S2-a and Fig. S2-b are close-up SEM images of Cu-Si nanolattice beam before and after lithiation with solid Li_2O electrolyte.

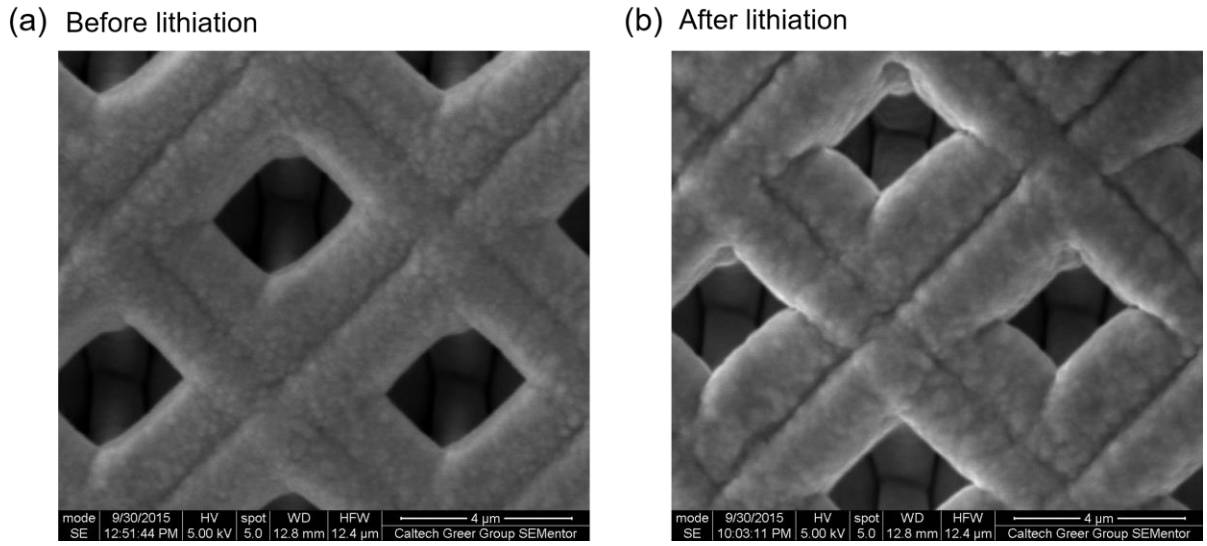

Figure S2. SEM images of Cu-Si nanolattice beams before and after lithiation with solid Li_2O electrolyte.

The volume expansion of each lithiated Cu-Si nanolattice was estimated by assuming a change in the cross-sectional area of the Si shell of the lattice, and by assuming that each beam does not elongate in the axial direction (Fig. S3). The minor and major axis of the cross-section of the Cu scaffold and the Cu-Si core-shell beam before and after lithiation were measured from SEM images for each nanolattice, and used in these calculations.

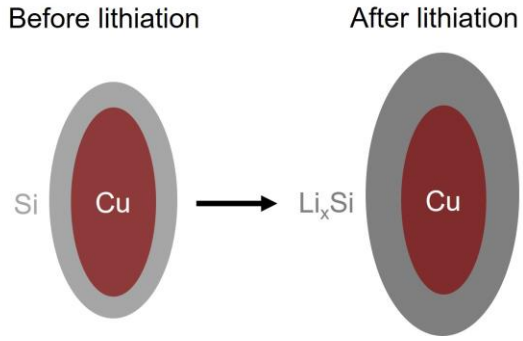

Figure S3. Illustration of Si volumetric expansion calculation from the Si shell cross-sectional area change.

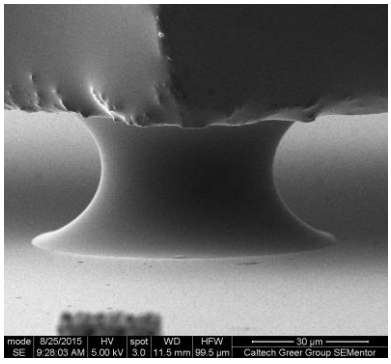

Figure S4. SEM image of the *in situ* half-cell with ionic liquid electrolyte after the Cu-Si nanolattice was fully immersed and the size of the ionic liquid droplet was stabilized.

Fig. S4 is a SEM image of the half-cell setup during the electrochemical characterization after the Cu-Si nanolattice was fully submerged and the size of the ionic liquid droplet was stabilized. Cyclical voltammetry was conducted between 0.01V and 2.5V at 2mV/s scanning rate inside SEM with the Cu-Si nanolattice and Li counter electrode using ionic liquid electrolyte (Fig. S5-a). The shape of the CV curve qualitatively agrees with that of Si lithiation but the anodic peaks were found to be at 0.71V and 1.20V instead of 0.37V and 0.62V reported in Ref. 1. We suspect the observed overpotential is possibly due to bad ion transport in the ionic liquid electrolyte and the internal resistance of the *in situ* setup.

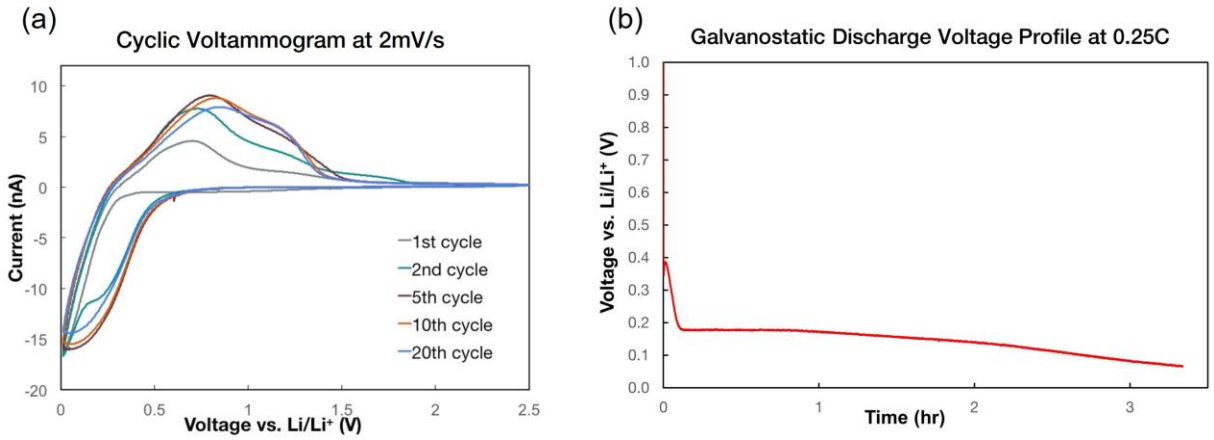

Figure S5. (a) Cyclic voltammogram for the *in situ* half-cell with the ionic liquid electrolyte at a voltage scanning rate of 2mV/s. (b) Galvanostatic discharge voltage profile of the *in situ* half-cell with the ionic liquid electrolyte at a discharge rate of ~0.25C.

Fig. S5-b displays a representative discharge voltage profile during a galvanostatic discharge at 10nA (~0.25C) with a 0.07V cutoff voltage. Via the combined motion of the sample stage and the nanomechanical arm, the suspended ionic liquid droplet was fine tuned to immerse the Cu-Si nanolattice structure with minimal contact between the substrate and the ionic liquid droplet in order to reduce the influence of Si thin film surrounding the nanolattice on measured electrochemical behavior. The area of the Si thin film on the substrate in contact with the ionic liquid also participated in the lithiation reaction and contributed to the total capacity. Therefore, the gravimetric specific capacity is normalized by the mass of Si in the nanolattice plus a 750nm-thick Si thin film disk of 70μm in diameter.

Simulation Section

Details of the fully-coupled diffusion-deformation finite element model, including the constitutive equations, boundary conditions and material parameter values, have been previously reported in Ref. 32. To adopt the model into the current system, the Cu core was modeled as linear elastic with a Young's modulus of 110GPa and a Poisson's ratio of 0.34. In Fig. 3a, the nodes on edge AC were prescribed zero horizontal displacement and zero Li flux, the nodes on edge CE were prescribed zero vertical displacement and zero flux. We prescribed a constant flux boundary condition on edge AE, with a magnitude of $J = (V/A) \cdot c_{max} \cdot C_{rate}/h$ where V and A are the volume and surface area of the a-Si shell, c_{max} is the maximum molar concentration of Li in the

Li-Si alloy, C_{rate} is the rate of discharge, and h = 3600s/hr is a unit conversion factor. Simulations were run until a normalized concentration of $c_{normalized} = c/c_{max} = 1$ was reached in any element of the mesh. The simulations were performed under plane strain conditions because the relatively high stiffness of the Cu, 110GPa, compared with that of the a-Si, 80GPa, effectively suppresses the out-of-plane expansion of the a-Si shell.

In order to determine the effects of using a plane-strain condition, we performed additional three-dimensional simulations. The simulations used only a single element in the out-of-plane direction (see Fig. S6), which we shall refer to as the z-direction. The bottom surface of this thin sheet (not visible in Fig. S6) is constrained to have zero displacement in the z-direction, while all of the nodes on the top surface with normal in the z-direction are constrained to have the same displacement in the z-direction. That is, the top surface is constrained to remain flat and all nodes must move in unison in the z-direction. This type of boundary condition is equivalent to modeling a long rod where any manner of end conditions (in this case the nodes of the nanolattice) is neglected.

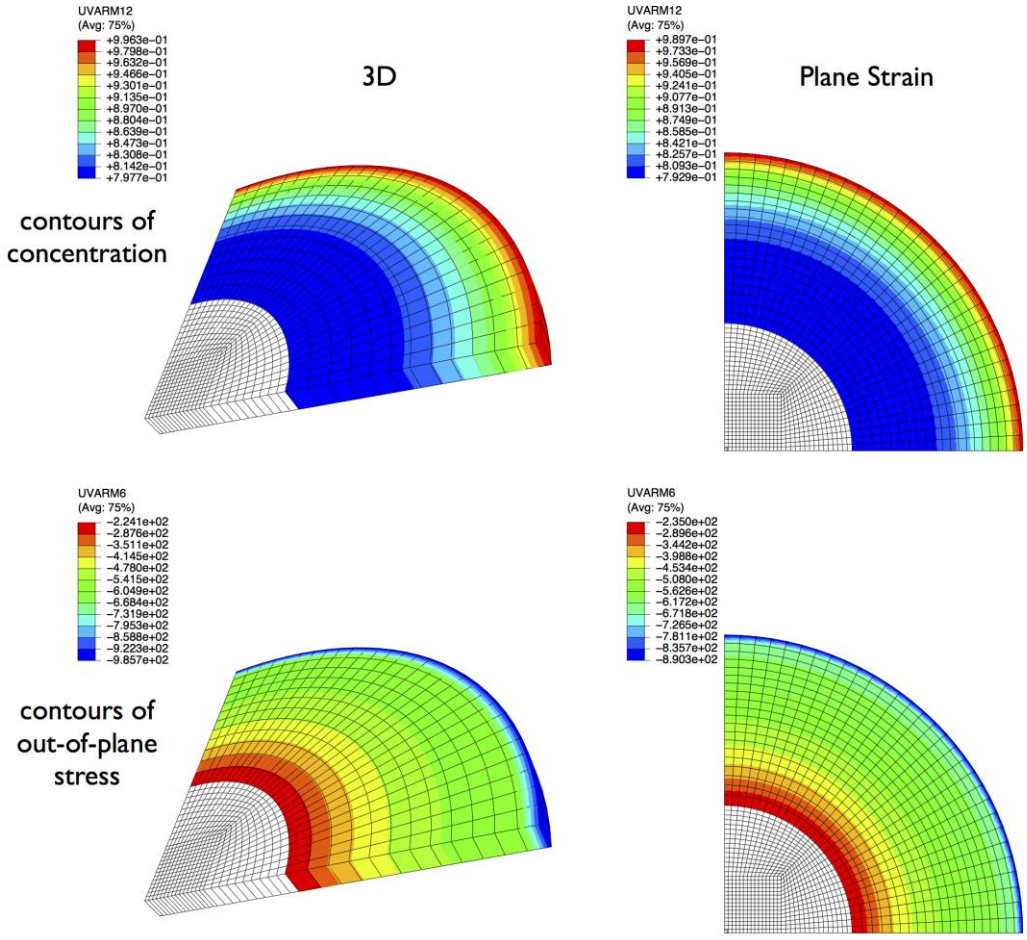

Figure S6. Comparison between a 3D simulation and a plane-strain simulation of the beam cross-section.

Figure S6 shows contours of normalized concentration (top) and out-of-plane stress σ_{zz} (bottom) for a 3D simulation (left) compared to a plane-strain simulation (right). As shown through these simulations, there is little effect in performing a plane strain simulation against a 3D simulation of

the form considered here. The reason for this is that the Cu core is relatively stiff compared to the a-Si shell and hence there is little out-of-plane displacement in the 3D simulations when the surface is constrained to remain flat. Of course, if one is to consider the entire nanolattice structure in a 3D simulation, the results, even at the center of one segment of the nanolattice, will be affected by the presence of the nodes.

In order to determine if fracture will occur in the a-Si shell during lithiation or delithiation we use the fracture energy measurements of Pharr et al. (Ref. 35). Since the maximum tensile stress in the a-Si shell during lithiation and delithiation cycles occur at low Li concentrations, we employed the fracture toughness of $\Gamma = 6.9 J/m^2$ which was measured experimentally by Pharr et al. at low Li concentrations (Ref. 35). Since we do not have good knowledge of the pre-existing flaws in the a-Si shell, following Xiao et al. (Ref. 34) and Pharr et al. (Ref. 35), we assumed that there is a through crack in the a-Si shell with length equal to initial thickness of the a-Si shell given by $h_f = 0.25\mu m$. The energy release rate G for a fully cracked film may be expressed as

$$G = g(\alpha, \beta)\frac{\sigma^2 h_f}{\bar{E}_f} \tag{1}$$

where $g(\alpha, \beta)$is a function of the Dundurs parameters, α and β, which are defined by

$$\alpha = \frac{\bar{E}_f - \bar{E}_s}{\bar{E}_f + \bar{E}_s}, \beta = \frac{\mu_f(1-2\nu_s) - \mu_s(1-2\nu_f)}{2\mu_f(1-\nu_s) + 2\mu_s(1-\nu_f)}$$

where $\bar{E} = E/(1-\nu^2)$ is the plane-strain modulus, and $\mu = E/(2(1+\nu))$ is the shear modulus (Ref. 36). For the a-Si shell, a Young's modulus $E_{Si} = 80GPa$ and a Poisson's ratio $\nu_{Si} = 0.22$ where used, and for Cu, a Young's modulus $E_{Cu} = 110GPa$ and a Poisson's ratio $\nu_{Cu} = 0.34$ was used. Using our calculated values of α and β, the tabulated values for $g(\alpha, \beta)$ found in Beuth (Ref. 36) were used to find $g = 1.28$ for our system. Finally, equating the energy release rate G with the experimentally measured fracture energy Γ, we are able to solve for $\sigma_c = 1.35GPa$.

Alternatively, we may compute the critical flaw size h_c for fracture to occur in a thin film through

$$h_c = \frac{2}{\pi}\frac{G\bar{E}_f}{\sigma^2} \tag{2}$$

by equating $G = \Gamma$ and using the maximum principal stress $\sigma = 0.71GPa$ measured during our lithiation simulations, as well as the aforementioned material properties (see Xiao et al. (Ref. 34) and Graetz et al. (Ref. 42)). The calculation yields a critical flaw size of $h_c \sim 700\ nm$, which is greater than the thickness of the a-Si shell prior to lithiation and after lithiation.

Given the stress profile obtained from FEA simulation, a simple Griffith model was adopted to estimate the Cu-Si interfacial delamination condition under normal and shear stresses. Suppose an internal crack of length 2a pre-exists at the Cu-Si interface possibly due to Si deposition flaw, the energy release rate G is a function of mode I and mode II stress intensity factor

$$G = \frac{1}{E^*}(K_I^2 + K_{II}^2) \tag{3}$$

where the effective elastic modulus $E^* = 2\left(\frac{1}{\bar{E}_{Cu}} + \frac{1}{\bar{E}_{Si}}\right)^{-1}$. As determined by Suo and Hutchinson (Ref. 37 and 38), for most bi-layer materials with reasonably small modulus mismatch, the complex stress intensity factor can be approximated as

$$K_I + iK_{II} = (\sigma_{22} + i\sigma_{12})\sqrt{2\pi a} \tag{4}$$

The fracture energy of the Cu-Si interface has been measured to be $\Gamma = 7.9J/m^2$ by Maranchi at al. (Ref. 39). According to Irwin (Ref. 40) and Griffith (Ref. 41), the crack will propagate only if the energy release rate G is greater than the fracture energy Γ. Using the maximum normal stress $\sigma_{max} = 0.74GPa$ and maximum shear stress $\tau_{max} = 0.27GPa$ from the simulation results at 1C, the critical crack length for delamination of the Cu-Si interface is $a_c = 203nm$.

We also performed a simulation including both lithiation and delithiation steps at 1C. The delithiation step began as soon as any element in the body reached a normalized concentration of one, and proceeded until any point in the body reached a concentration of 1%. Similar to Fig. 3c and 3d, Fig. S7 shows the interfacial normal stress and shear stress at the Cu-Si interface. For the normal stress (left) we note that the interfacial stresses during delithiation are mainly compressive, and hence would not be expected to cause delamination. For the shear stress (right), we noted that the magnitude of the maximum interfacial shear stress during delithiation is lower than that during lithiation. Hence, delithiation is not likely to lead to failure at the Cu-Si interface.

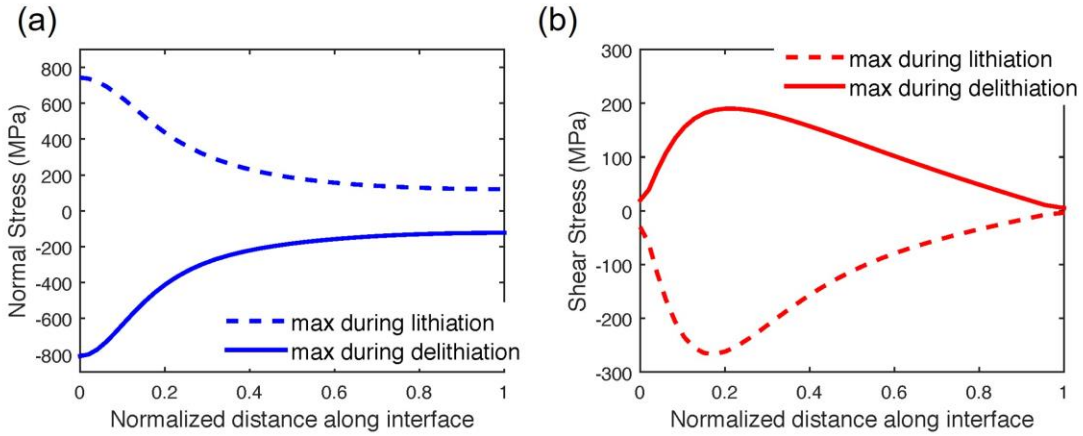

Figure S7. Distribution profile of the maximum interfacial (a) normal and (b) shear stress during lithiation and delithiation calculated by finite element modelling.

However, during delithiation, the maximum principal stress was shown to be tensile on the exterior free surface of the Si shell. Fig. S8 shows contours of maximum principal stress at the start, middle, and end of the delithiation step. As shown in Fig. S8, this stress can reach a level of $\sigma = 1.70GPa$ at low concentrations. This value is greater than the critical stress $\sigma_c = 1.35GPa$ computed in our earlier analysis, hence it is possible that fracture can occur in the a-Si shell during deliathion. The critical flaw size $h_c$which would cause such failure can be computed using the value of the maxmimum principal stress $\sigma = 1.70GPa$ and the eq. (2) and is equal to $h_c = 127nm$. It is possible but quite unlikely that such a flaw is present in a-Si as it is roughly half the thickness of the original a-Si shell prior to lithiation. We did not observe such prominent flaws in

the TEM samples, and no surface cracks were observed during *in situ* SEM delithiation experiments at a delithiation rate of ~0.25C.

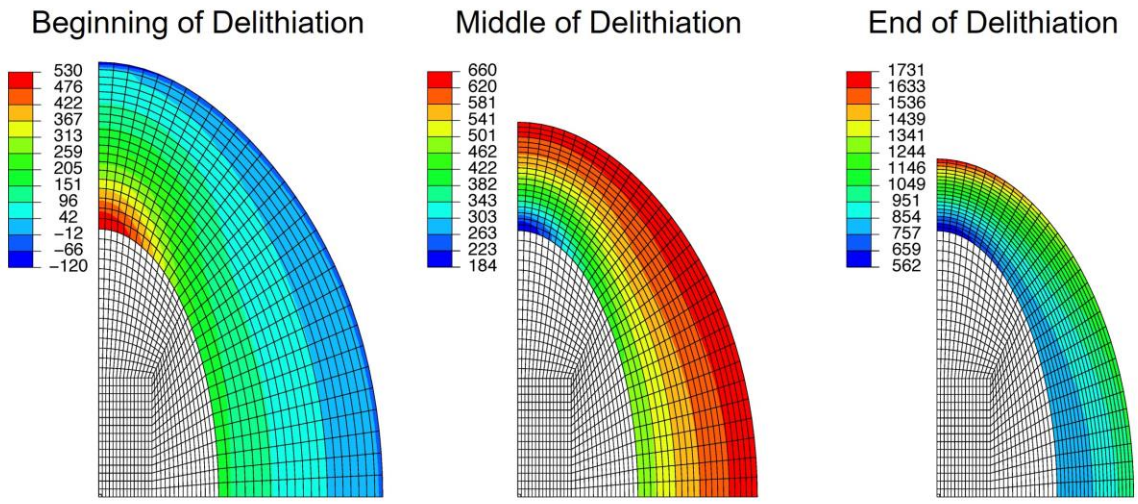

Figure S8. Contours of the maximum principal stress of the a-Si shell in the beginning, middle and final stage of delithiation.